Advances in Nano Research, *Vol. 10, No. 3 (2021) 253-261*
DOI: https://doi.org/10.12989/anr.2021.10.3.253

Nanoscale quantitative mechanical mapping of poly dimethylsiloxane in a time dependent fashion

Shuting Zhang*, Yu Ji and Chunhua Ma**

Collaborative Innovation Center of Henan Province for Green Manufacturing of Fine Chemicals, Key Laboratory of Green Chemical Media and Reactions, Ministry of Education, School of Chemistry and Chemical Engineering, Henan Normal University, Xinxiang, Henan 453007, China

(*Received June 7, 2020, Revised December 7, 2020, Accepted December 10, 2020*)

Abstract. Polydimethylsiloxane (PDMS) is one of the most widely adopted silicon-based organic polymeric elastomers. Elastomeric nanostructures are normally required to accomplish an explicit mechanical role and correspondingly their mechanical properties are crucial to affect device and material performance. Despite its wide application, the mechanical properties of PDMS are yet fully understood. In particular, the time dependent mechanical response of PDMS has not been fully elucidated. Here, utilizing state-of-the-art PeakForce Quantitative Nanomechanical Mapping (PFQNM) together with Force Volume (FV) and Fast Force Volume (FFV), the elastic moduli of PDMS samples were assessed in a time-dependent fashion. Specifically, the acquisition frequency was discretely changed four orders of magnitude from 0.1 Hz up to 2 kHz. Careful calibrations were done. Force data were fitted with a linearized DMT contact mechanics model considering surface adhesion force. Increased Young's modulus was discovered with increasing acquisition frequency. It was measured 878 ± 274 kPa at 0.1 Hz and increased to 4586 ± 758 kPa at 2 kHz. The robust local probing of mechanical measurement as well as unprecedented high-resolution topography imaging open new avenues for quantitative nanomechanical mapping of soft polymers, and can be extended to soft biological systems.

Keywords: polydimethylsiloxane (PDMS); PeakForce quantitative nanomechanical mapping (PFQNM); fast force volume (FFV); Young's modulus; DMT model; atomic force microscopy (AFM)

1. Introduction

Polydimethylsiloxane (PDMS) is one of the most widely adopted silicon-based organic polymeric elastomers. Due to its biocompatibility, optical transparency, low auto-fluorescence, cost effective, ease of fabrication and flexible moldability (Lee *et al*. 2003, Mata *et al*. 2005, McDonald and Whitesides 2002, Piruska *et al*. 2005, Sia and Whitesides 2003), PDMS has been extensively applied in the research fields of cell physiology (Chuah *et al*. 2015, Punjabi *et al*. 2018), drug release (Kim *et al*. 2006), drug delivery (Ziaie *et al*. 2004), biosensors (Wu *et al*. 2015), microfluidic device (Fujii 2002), material science (Cortese *et al*. 2008). Elastomeric nanostructures are normally required to accomplish an explicit mechanical role and correspondingly their mechanical properties are crucial to affect device and material performance (Ebrahimi *et al*. 2019, Johnston *et al*. 2014). Despite its wide application, the mechanical properties of PDMS are yet fully understood. The elastic modulus measurement of soft polymers, such as PDMS remains a major challenge for a number of reasons. Firstly, PDMS, depending on crosslinking and curing process, can be viscoelastic. Secondly, large surface forces exist that complicate the indentation process. Thirdly, there is a lack of robust model that faithfully predicts contact mechanics. Much effort has been made to explore the mechanical properties of PDMS. Notable progress has been achieved to understanding the elastic modulus of PDMS. For examples, how fabrication process (Johnston *et al*. 2014), dimensions (Liu *et al*. 2009), curing temperature (Johnston *et al*. 2014) and mix ratio of cross-linking agents (Carrillo *et al*. 2005) affect Young's modulus have been delineated. However, the vast majority of studies on bulk scale using ensemble mechanical instruments do not satisfy the growing interest in nanoscale mechanical characterization. Many researchers have resorted to other techniques, such as Atomic Force Microscopy (AFM).

Ever since its advent, AFM has progressed to a powerful tool in high resolution imaging regardless of medium (Binnig *et al*. 1986). Owing to the contact nature and large vertical deflection feedback, contact mode AFM imaging suffers large unwanted shear force and vertical load that are invasive for both tip and sample. Tapping mode AFM imaging circumvents the shear force by vertically vibrating the cantilever. It requires a stiff cantilever and tries to keep the cantilever vibration amplitude constant that still indirectly yields high tapping force (Bensaid 2017, Vahdat *et al*. 2013). In recent years, a novel imaging mode called PeakForce Tapping (PFT) has emerged (Xu *et al*. 2018). It

*Corresponding author, Professor,
E-mail: szhang2017@126.com
**Co-corresponding author, Professor,
E-mail: xiaoma3625@126.com

ISSN: 2287-237X (Print), 2287-2388 (Online)

taps in such a way that the *Z* piezo moves the whole probe holder up and down at low frequencies, normally in the range of 0.5 kHz to 2 kHz. It has superior control over force since it has direct feedback on vertical deflection of the cantilever. Moreover, it still preserves high resolution as well as low invasiveness. These features make PFT a suitable technique in topography imaging of soft biological specimen and polymer samples. For instance, peak force tapping mode has been successfully applied to visualizing soft and flexible microvilli structure on epithelial cell surface, which had previously been unable to achieve (Schillers *et al*. 2016). It has also been used to investigate the adhesion force between conducting polymers (Liu *et al*. 2015) and biorecognition event at the single molecule level (Kang *et al*. 2019).

Besides topography imaging, AFM is an excellent tool to explore samples' mechanical properties. Conventionally, AFM is capable of monitoring vertical deflection change when ramping *Z* piezo position. The force load and unload curves are recorded and fitted with different models based on contact mechanics. It can be done either in a single point measurement or in a location array fashion, so called Force Volume (FV). The major drawback of conventional force measurement is its slow sampling because the rate is intrinsically limited by the instrument. The PFT based Quantitative Nanomechanical Mapping (PFQNM) is an emerging approach that takes advantage of mapping mechanical properties and imaging sample topography simultaneously. So far, PFQNM has been broadly utilized to characterize the mechanical properties of a wide range of materials, including hardened cement paste (Trtik *et al*. 2012), living cells (Krieg *et al*. 2019), amyloid fibrils (Adamcik *et al*. 2011), polymer matrix composite (Fard *et al*. 2020) and a variety of polymers (Young *et al*. 2011). Along with it, high resolution height image is also collected, making it convenient to correlate mechanical properties with sample topography at the nanoscale. For instance, a recent rigorous PFQNM study by Germanicus and coworkers have taken this advantage and successfully imaged silica beads embedded in an epoxy resin matrix and measured their elastic modulus (Germanicus *et al*. 2020). The measured modulus was in between 62-84 GPa. The authors have demonstrated and expanded the capability of PFQNM measurement on very stiff materials. PFQNM and regular force volume are complimentary. However, there is still a rate gap in between, as PFQNM works in the range of 125 Hz to 2 kHz and regular force volume performs only as slow as a few hertz. A method named Fast Force Volume (FFV) has filled this gap. It can be operated from slower than 1 Hz up to about 140 Hz. The underlying working mechanism for fast force volume lies in the smoothing of triangular drive signal, resulting in fast turnaround between force curves. Therefore, PFQNM, force volume together with fast force volume cover four orders of magnitude in terms of force loading/unloading rate. They can be employed to investigate time dependent mechanical properties, such as those for soft polymers.

Although several lines of attempts have been reported using AFM nanoindentation on mechanical measurement of PDMS (Kim *et al*. 2008, Sarrazin *et al*. 2016), the time dependent mechanical response of PDMS has not been fully elucidated. In this study, the elastic moduli of a PDMS sample was assessed in a time-dependent fashion. Specifically, the ramp frequency changed discretely from 0.1 Hz up to 2 kHz. Rigorous calibrations were done, and data were fitted with a proper DMT contact mechanics model. Increasing Young's modulus was discovered with increasing ramp frequency. The robust mechanical measurement as well as unprecedented high resolution topography imaging open new avenues for quantitative nanomechanical mapping of soft polymers, and can be extended to soft biological systems.

2. Materials and methods

2.1 Materials

A PeakForce QNM sample kit was purchased from Bruker Co. (Santa Barbara, CA). The kit contains a PDMS sample, a sapphire sample and a tip check sample. ScanAsyst-Air probes were acquired from Bruker Co. (Santa Barbara, CA) with nominal spring constant of 0.4 N/m. The probes were coated with aluminum on the cantilever back side to enhance laser deflection.

2.2 PDMS preparation

PDMS elastomer samples were prepared by mixing a pre-polymer base (part A) and a cross-linking curing agent (part B) at ratio of 5:1 (Sylgard 184 Elastomer 184, Dow Corning Corp. Midland, MI). The solution was stirred for 15 min, followed by pouring into a flat bottom polystyrene dish. Air bubbles were removed by degassing when placed under vacuum. The PDMS sample was let cure at room temperature for 48 hrs. After curing, the PDMS network samples were cut out into 1 cm square and about 1 mm in thickness with a stainless scalper. The PDMS samples were then mounted on metal pucks (Ted Pella Inc., Redding, CA) using double-sided tape.

2.3 Calibrations

A Dimension ICON AFM (Bruker Co., Santa Barbara, CA) with built in ScanAsyst mode was employed to do calibrations and mechanical measurements. Force ramp and force volume required calibrations on cantilever deflection sensitivity, cantilever spring constant and tip radius. Three probes were used in this study. The calibration procedures were as the following. Cantilever deflection sensitivity was calibrated by so called touch calibration approach, in which a ScanAsyst-Air probe is engaged onto a very hard surface, in this case a sapphire sample, to do a force ramp. The ramp output was selected for *Z*. Ramp size was set at 300 nm and the trigger threshold was defined at 0.5 V above the baseline background. After a force-displacement curve was collected, a pair of lines were used to cover the most linear part of the contact region. The deflection sensitivity would be automatically calibrated and updated once updating deflection sensitivity. The measured deflection sensitivity

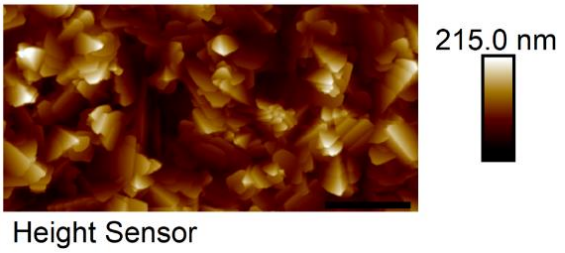

Fig. 1 Height image of the tip check sample scanned by a ScanAsyst-Air probe. The scale bar in *x* axis represents 600 nm. *Z* scale is 215 nm

was 64.7 ± 8.2 nm/V (n = 3). Next, thermal tune was performed to collect the thermal spectrum of the cantilever vibration in free air. The vibration frequency peak could be fitted and found by the real time NanoScope software that was provided by the AFM manufacturer (Bruker Co. Santa Barbara, CA). According to the theory of equipartition theorem

$$\frac{1}{2}k_B T = \frac{1}{2}kd^2 \quad (1)$$

where k_B is the Boltzmann constant, T is the temperature in Kelvin, and d is the root mean square value of the cantilever vibration. A correction factor at 1.09 was taken into account and the spring constant k was calculated accordingly. Tip radius was estimated by carefully scanning the probe across the tip check sample (Fig. 1). The sample was made of titanium that has sharp ends at some parts. At each sharp end, it captured a piece of tip shape. Altogether, they could be used to reconstruct the tip shape, which was assumed to be a sphere. An indentation depth was needed to accurately estimate the tip radius. The indentation depth (13.3 ± 2.4 nm, n = 3) was obtained by measuring the distance between the zero separation and the lowest point in adhesion force. The number was substituted in the Height from apex on the tip check image. An effective tip radius was thereby calibrated.

PFQNM measurements required two more parameters to be calibrated. They were Sync Distance and PFT Amplitude Sensitivity. Sync distance is a time constant at which the Z piezo reaches the lowest position. PFT amplitude sensitivity is a scaling factor that governs how the digitally input drive signal transfers to the physically Z piezo output. Its calibration ensures user has the accurate Z piezo displacement as desired. Both sync distance and PFT amplitude sensitivity were calibrated on a sapphire sample using touch calibration. Notably, the sync distance and PFT amplitude sensitivity are frequency dependent. Both are required to be calibrated at discrete frequencies until reach the desired condition. In this work, a series of frequencies were selected in the range of 0.125-2 kHz.

2.4 PFQNM quantitative nanomechanical mapping

ScanAsyst-Air probes were loaded for quantitative nanomechanical mapping of the PDMS sample. The calibrated spring constants fell in the range of 0.2-0.8 N/m.

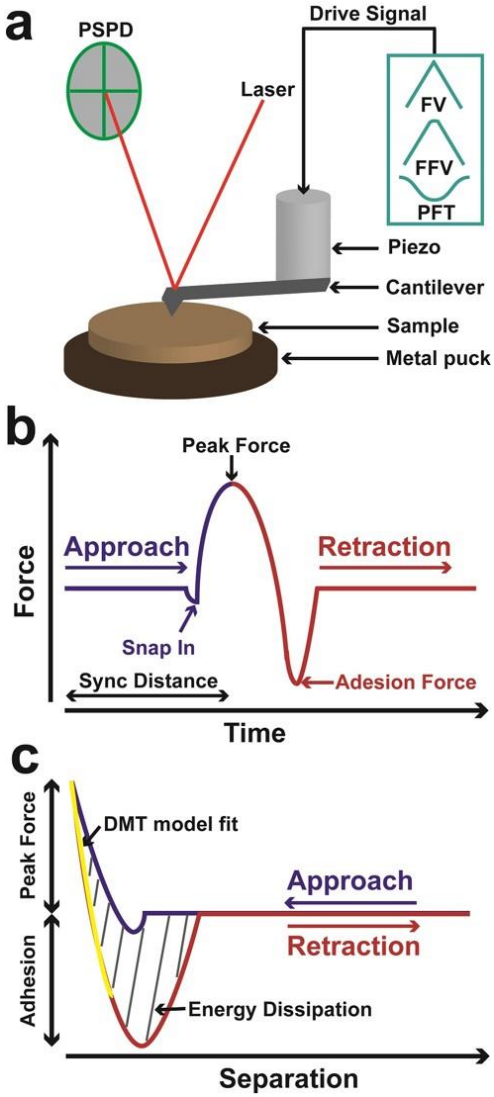

Fig. 2 Experimental design, data collection and force analysis. The PDMS sample was mounted onto a metal puck. A sharp cantilever indented into the PDMS sample and retracted away when a well define applied force was reached (Fig. 1(a)). A laser shined and bounced off the cantilever. The deflection signal was received by PSPD. The cantilever movement was controlled by the Z piezo. Depending on the technique, it could be a triangular wave (FV), a rounded triangular wave (FFV) or a sine ware signal (PFQNM). The PFQNM was schematically illustrated in Fig. 1(b), force versus time curve clearly showed the tip had a snap-in contact when approaching the sample surface and a snap-out of contact when retracting away from the sample surface. The sync distance is a time constant when the Z piezo reaches the lowest point. AFM recorded the force versus Z displacement curve and was further converted into the force versus tip-sample separation curve (Fig. 1(c)). The DMT modulus was extracted by fitting the retraction curve with DMT. The energy dissipation was calculated by integrating the hysteresis loop

Upon scanning, the force setpoint was set at 100 pN. The imaging acquiring rate (scan rate), feedback gain and Z range were automatically adjusted by the ScanAsyst auto control, an automation feature of the ScanAsyst mode. The samples per line and number of lines were both kept at 256, meaning digital resolution was 256 × 256. The PFT frequency was varied from 2 kHz to 0.125 kHz among experiments to give rise to time dependent force loading and unloading. For 2 kHz PFT frequency and 100 nm PFT amplitude, the corresponding force loading rate was 0.8 mm s^{-1}. The Poisson's ratio for viscoelastic PDMS was assumed to be 0.5 (Carrillo *et al*. 2005). A 5 μm × 5 μm region was imaged simultaneously with topography and mechanical measurements. The NanoScope control software had large bandwidth to compute mechanical data and display them in real time channels. Those data were saved in raw images for further offline analysis. In the end, a number of image channels were saved, including height sensor, DMT modulus, adhesion map, indentation and energy dissipation channels. To verify the high spatial resolution of PFQNM, a 2 μm × 2 μm scan was also performed.

2.5 AFM force ramp and fast force volume

Force ramp and fast force volume were conducted by ramping *Z* piezo displacement while recording vertical deflection of cantilever. The ramp size was 200 nm. Low trigger force setpoint at 100 pN was achieved by a constant background subtraction that ensures the deflection drift was excluded during ramp process. Again, a sampling array was defined over a 5 μm × 5 μm region. The ramp rates were 0.1 Hz, 1 Hz, 10 Hz, 20 Hz, 61 Hz and 122 Hz. For 1 Hz ramp rate and 200 ramp size, the corresponding force loading rate was 400 nm s^{-1}. The ramp curves were collected at 8 × 8 for 0.1 Hz, 16 × 16 for 1 Hz, 64 × 64 for 10 Hz, 128 × 128 for 20 Hz, 61 Hz and 122 Hz.

2.6 Experimental setup

In order to quantitatively measure the elastic modulus of the PDMS sample (Fig. 2), the experiment was set up in such a way that a sharp cantilever indented into the PDMS sample and departed off until a well define applied force was reached (Fig. 2(a)). The force was detected by monitoring the laser deflection signal in the Position Sensitive Photodiode (PSPD). The cantilever movement was controlled by the *Z* piezo. Depending on the technique, it could be a triangular wave (FV), a rounded triangular wave (FFV) or a sine ware signal (PFQNM). The PFQNM was schematically illustrated in Fig. 2(b), force versus time curve clearly showed the tip had a snap-in contact when approaching the sample surface and a snap-out of contact when retracting away from the sample surface. The sync distance is a turning point that separates approach and retraction curves. On a hard surface, this point is a time constant when the *Z* piezo reaches the lowest position. It also means the force reaches the peak force at the time point. On a soft compliant sample, this point could shift a little due to time dependent sample deformation. Regardless of the techniques adopted, AFM recorded the force versus *Z* displacement curve and was further converted into the force versus tip-sample separation curve (Fig. 2(c)). The retraction curve was fitted with the linearized DMT model and the DMT modulus is extracted. The energy dissipation was calculated by integrating the hysteresis loop. Cantilever spring constant had to be chosen prudently so that the probe tip will be able to indent into the sample while it still has enough force sensitivity to be recorded by AFM instrumentation. Cantilever spring constant alone did not dictate the probe selection. Another factor that needed to be considered was the tip radius as applied stress by tip also dependent on contact area. In the present work, ScanAsyst-Air probes were selected because it has high force sensitivity so the applied force can be precisely controlled. All force measurements were carried out three independent times. Results were reported in the form of mean ± SD (standard deviation) while number of independent experiments were reported as $n = 3$.

2.7 Data analysis

Force versus *Z* piezo displacement (F-Z) curves were collected for force ramp, fast force volume and PFQNM. Z piezo displacement consists of three components, namely tip-sample separation (D), cantilever deflection (d) and indentation depth (δ). Force versus tip-sample separation (F-D) curves are physically meaningful and imperative for model fit. Subtracting cantilever deflection (d), and indentation depth (δ) from Z can be done either in real time control software or by offline data analysis software, providing the cantilever deflection sensitivity and spring constant have been calibrated. In addition, the force curve baseline was offset to zero with baseline correction function. Finally, F-D curves were obtained and subject to DMT model fit. Base on the Hertzian contact theory

$$F_{app} = \frac{4}{3} E_r \sqrt{R} \delta^{\frac{3}{2}} + F_{adh} \tag{2}$$

where F_{app} is the applied force tip exerted on the sample (Eltaher *et al*. 2019). Adhesion force (F_{adh}) is taken into account. R is the tip radius for a sphere tip. δ is the indentation depth. E_r is the reduced Young's modulus. It is related to tip and sample

$$\frac{1}{E_r} = \left(\frac{1 - v_s^2}{E_s}\right) + \left(\frac{1 - v_t^2}{E_t}\right) \tag{3}$$

where v_s and v_t are the Poisson's ratios of sample and AFM tip respectively. E_s and E_t are the Young's moduli of sample and AFM tip, respectively. The tip's Young's modulus of several orders of magnitude larger than that of the PDMS sample, so the tip term can be neglected. Once E_r and v_s are known, E_s can be readily calculated.

By taking both sides of Eq. (2) to the 2/3 power after subtracting the F_{adh} from F_{app}, a linearized model has been employed to fit all force data (Carl and Schillers 2008). This model does not require identification of contact point.

$$\left(F_{app} - F_{adh}\right)^{\frac{2}{3}} = \left(\frac{4}{3} E_r \sqrt{R}\right)^{\frac{2}{3}} \delta \tag{4}$$

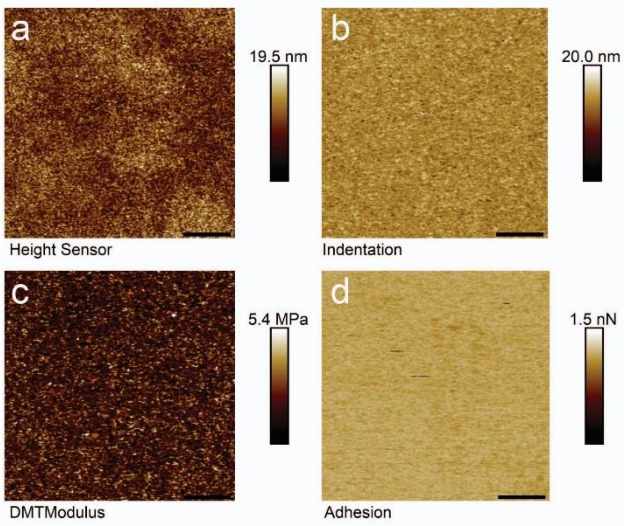

Fig. 3 Representative PFQNM nanomechanical mapping (5 μm × 5 μm) of PDMS sample at 2 kHz. Panels (a)-(d) are height sensor image, indentation channel, DMT modulus channel and adhesion force mapping. For all images, the scale bar represents 1 μm. The Z scales for channels (a)-(d) are 19.5 nm, 20 nm, 5.4 MPa, and 1.5 nN, respectively. Surface roughness of the height sensor image was reported in the form of R_q as 2.84 ± 0.11 nm (n = 3).

Then E_r and E_s were extracted as a result.

$$E_r = \frac{3}{4}\left(\frac{\left(F_{app} - F_{adh}\right)^{\frac{2}{3}}}{\delta}\right)^{\frac{3}{2}} \frac{1}{\sqrt{R}} = \frac{3}{4}\text{slope}^{\frac{3}{2}} \frac{1}{\sqrt{R}} \quad (5)$$

The applied force was calculated from Hooke's law since cantilever acted like a spring.

$$F_{app} = k \times d \quad (6)$$

where k is the cantilever spring constant and d is the cantilever deflection, which was obtained from multiplying cantilever deflection sensitivity with deflection signal.

Offline data analysis was conducted with the NanoScope Analysis software (Bruker Co., Santa Barbara, CA) supplied by the AFM factory. All topographical images were subject to first order flatten that gets rid of drift, background noise as well as correcting sample tilt. The surface roughness was evaluated by surface roughness feature provided by the NanoScope Analysis software.

$$R_q = \sqrt{\frac{\sum(Z_i - Z_m)^2}{N}} \quad (7)$$

where N is the total number of points within the image area, Z_i is the Z height of the i^{th} data point, and Z_m is the mean Z height over the whole area. All mechanical data images were left intact without levelling.

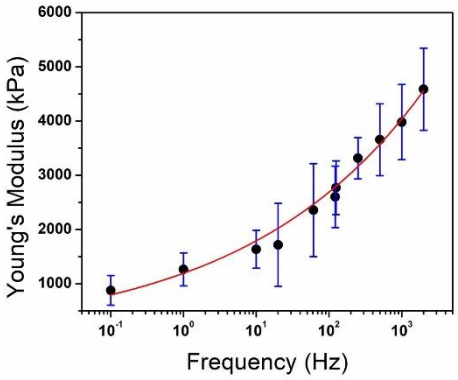

Fig. 4 Relationship between measured Young's modulus (E) and the force mapping frequency (f). The measured Young's moduli at different frequencies were tabulated in Table 1. The data were fitted with a power function yielded $E = 1192.88 \times f^{0.18}$ ($R^2 = 0.99$)

Table 1 Measured Young's modulus at different frequencies

Frequency (Hz)	Modulus (kPa, mean ± SD)
0.1	878 ± 274
1	1266 ± 304
10	1635 ± 349
20	1717 ± 766
61	2358 ± 858
122	2602 ± 566
125	2770 ± 497
250	3315 ± 380
500	3656 ± 663
1000	3981 ± 693
2000	4586 ± 758

3. Results

The modulus mapping data, along with height, indentation and adhesion mapping, were assembled in Fig. 3. The elastic moduli at different mapping frequencies were pooled together (Fig. 4). Young's moduli data were reported in Table 1. Data points of mechanical mapping at each frequency was noted as n. The Young's moduli at 0.1 Hz, 1 Hz, 10 Hz, 20 Hz, 61 Hz, 122 Hz, 125 Hz, 250 Hz, 500 Hz, 1 kHz and 2 kHz were 878 ± 274 kPa (n = 3), 1266 ± 304 kPa (n = 3), 1635 ± 349 kPa (n = 3), 1717 ± 766 kPa (n = 3), 2358 ± 858 kPa (n = 3), 2602 ± 566 kPa (n = 3), 2770 ± 497 kPa (n = 3), 3315 ± 380 kPa (n = 3), 3656 ± 663 kPa (n = 3), 3981 ± 693 kPa (n = 3), 4586 ± 758 kPa (n = 3), respectively. The scatter plot was generated with Origin 8.5 software. The data were fitted with a power function yielded $E = 1192.88 \times f^{0.18}$ ($R^2 = 0.99$). Representative PFQNM nanomechanical mapping (2 μm × 2 μm) of PDMS sample at 2 kHz was shown in Fig. 5. There was some shift in adhesion force in the bottom-right of Fig. 5(d), possibly because of poor crosslinking during sample preparation or sample degradation that changed sample integrity

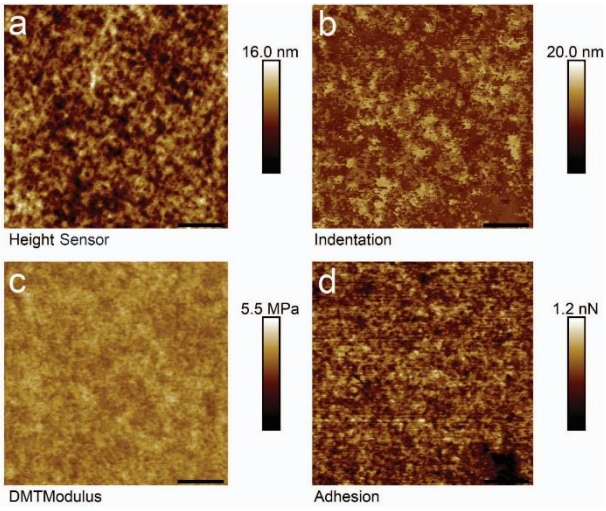

Fig. 5 Representative PFQNM nanomechanical mapping (2 μm × 2 μm) of PDMS sample at 2 kHz. Panels a-d are height sensor image, indentation channel, DMT modulus channel, and adhesion force mapping. For all images, the scale bar represents 0.4 µm. The *Z* scales for channels (a)-(d) are 16 nm, 20 nm, 5.5 MPa and 1.2 nN, respectively. Surface roughness of the height sensor image was reported in the form of R_q as 2.11 ± 0.07 nm

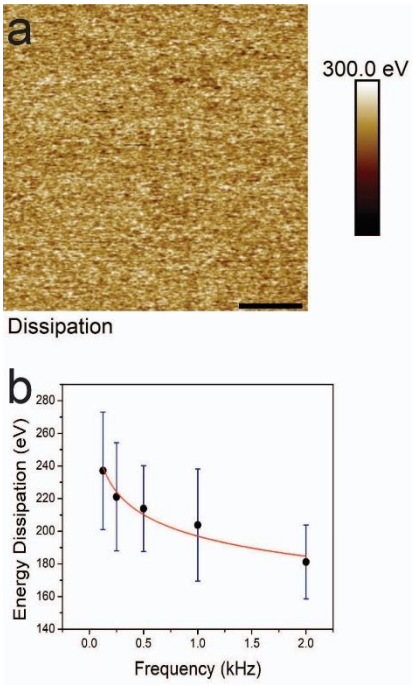

Fig. 6 Representative energy dissipation mapping image at (a) 2 kHz. The relationship between energy dissipation (E_{diss}) and different mapping frequencies (f) was shown in (b). The energy dissipation values obtained at 2 kHz, 1 kHz, 0.5 kHz, 0.25 kHz and 0.125 kHz were 181.2 ± 22.6 eV, 203.8 ± 34.3 eV, 213.9 ± 26.3 eV, 221.1 ± 33.2 eV, 237.1 ± 36 eV, respectively. The data were fitted with a power function yielded $E_{diss} = 197.02 \times f^{-0.09}$ ($R^2 = 0.94$)

locally. The relationship between energy dissipation and different mapping frequencies was plotted in Fig. 6. The energy dissipation values obtained at 2 kHz, 1 kHz, 0.5 kHz, 0.25 kHz, and 0.125 kHz were 181.2 ± 22.6 eV (n = 3), 203.8 ± 34.3 eV (n = 3), 213.9 ± 26.3 eV (n = 3), 221.1 ± 33.2 eV (n = 3), 237.1 ± 36 eV (n = 3), respectively. The data were fitted with a power function yielded $y = 197.02 \times x^{-0.09}$ ($R^2 = 0.94$).

4. Discussion

The Hertz model is a widely adopted contact mechanics model (Shi and Zhao 2004). It describes the scenario when a rigid probe indents a semi-infinite, isotropic, homogeneous elastic surface. However, the Hertz model assumes no surface forces, which exist for soft materials. Incorporating surface forces, both the Johnson-Kendall-Roberts (JKR) model and the Derjaguin-Muller-Toporov (DMT) model have been developed. While the JKR model is suitable for low elastic modulus, high adhesion and large tip radius systems where there are short rang surface forces, the DMT model can be implemented to high elastic modulus, low adhesion, and small tip radius systems where there are long rang surface forces. Protocol for force curve acquisition and model for data analysis are justified. In current investigation, the force setpoint at 100 pN has been empirically acquired, and verified to be the optimum value in terms of getting meaningful indentation depth while the DMT model still holds. Low force load also leads to sample deformation in elastic regime not plastic regime. Despite the existence of adhesion force, the force-indentation still majorly follows linear stress-strain relationship. In addition, sharp tip enables high resolution sample topography imaging in PFQNM measurements, which is an attractive advantage when correlates sample topography with mechanical properties. Taken together, the current experiment setup fulfills the DMT model. Previously studies have shown that PDMS membranes behavior differently when they are thicker than 200 µm, compared with the ones below 200 µm (Liu *et al*. 2009). The thickness dependent Young's modulus change is attributed to the reordering of polymer chains during fabrication of thin layers. The Hertz assumption of infinitesimal deformation is valid in the present setup according to Dimitriadis *et al*. (2002) who introduced a dimensionless parameter $\chi = \sqrt{R\delta}/h \leq 1$, where h is the sample thickness.

Tip radius estimation is not trivial in quantitative mechanical measurements. Many researches ballpark the tip radius by backward estimating using a sample with known tip radius (Young *et al*. 2011, Zeng *et al*. 2018). This work adopts a different reconstruction strategy that does not require such a sample. It has been documented that using blunt tips tend to yield tighter modulus numbers and that sharp tips may overestimate the modulus. The moduli of PDMS here are indeed slightly higher than reported in literature where samples were prepared similarly (Cao *et al*. 2005, Sarrazin *et al*. 2016, Wang *et al*. 2015). However, sharp tips preserve high spatial resolution (see a 2 μm × 2

μm scan in Fig. 5), an advantage not possessed by other techniques. Sharp tips, even under small load, can penetrate into compliant samples due to large stress, resulting in large indentation. Therefore, it could compromise the validity of the DMT model. That is not the case in this study as the applied force is controlled in a precise and sensitive manner, evidenced by the resulted indentation depth and the effective tip radius in the same order of magnitude (14.8 ± 3.7 nm, n = 3). Large tip radius, however, can be instrumental in case of measuring elastic modulus on stiff materials. A recent study has utilized a calibration grating sample to estimate hand-crafted diamond tips with steel cantilevers (Germanicus *et al*. 2020). The authors have estimated the tip radii around 60 nm and were able to apply them on silica beads in epoxy matrix with PFQNM. The large and stable contact between the tip and the sample has ensured elastic deformation of the silica beads sample. Surface roughness (R_q) of the PDMS height image is 2.84 ± 0.11 nm, indicating the surface is flat and surface roughness should not be treated as a confounding factor to quantitative measurements (Carrillo *et al*. 2005). Fig. 5(b) shows some locations display higher indentation depth than the rest. This could be caused by unstable contact between the tip and the edge of the PDMS features (Germanicus *et al*. 2020). It means the PDMS sample has certain non-uniformity at the nanometer scale, as shown in the heigh sensor image (Fig. 5(a)). In addition, the linearized DMT model fit does not require determination of the contact point that could otherwise lead to major errors in the final calculated modulus (Hellwig *et al*. 2017).

Tuning the mechanical properties of PDMS has tremendous effect on biomedical and nanomaterials research. Xin *et al*. (2018) have discovered that PDMS substrates with different Young's moduli mediate cell response, in particular the long-term cell growth (Brown *et al*. 2005, Reyes *et al*. 2017, Villanueva-Cab and Pal 2017). The present work shows that increasing force loading/unloading rate increases Young's modulus. This finding is in line with a finding from previous experiment by Wang et al, in which they used nanoindentation Dynamic Mechanical Analysis (nDMA) and demonstrated the frequency dependent storage modulus shifting of PDMS (Wang *et al*. 2015). Storage modulus, the elastic portion of the stored energy, is not elastic modulus per se. Nevertheless, PDMS is viscoelastic and response time plays an important role. This is supported by the energy dissipation mapping, an observable that explicitly demonstrates how much energy loss per tapping cycle (Fig. 6). The more viscoelastic of the material, the more energy loss it incurs. While large probe-based AFM nano-indentation measures elastic modulus of soft samples as a whole, it does not possess high spatial resolution of elasticity. Such local mechanical properties are essential for some specimen. For instance, cells are composed of various substructures like cytoskeleton, filament network and microvilli, exhibiting different elasticities (Carl and Schillers 2008). A remarkable note from the study is that FFV transitions smoothly into PFQNM frequency regime, no pronounced deviation of modulus data was observed (Fig. 4). It is plausible that FFV combined with PFQNM can be implemented in mechanical mapping of soft complex biological systems (Supraja *et al*. 2018). A recent paper has studied the elastic modulus of fibroblast cells in the frequency range of 0.3 Hz-250 Hz (Efremov *et al*. 2019). Although it is on living cells, the authors have reported raised apparent Young's modulus when increasing the ramp frequency, consistent with the finding of current work. The approach reported here is as reliable as any other nanomechanical techniques provided the force-indentation has been prudently designed and the data analysis has been carefully executed. Furthermore, the PFQNM part is advantageous over traditional AFM nanoindentation in terms of local probing of mechanical properties. A recent study by Fard *et al*. (2020) have successfully implemented PFQNM on high resolution topography imaging together with modulus mapping on through-thickness interphase in polymer matrix composites. They have discovered that long-term exposure to heat and humidity causes hygro-thermal induced stress, interface debonding, and causes damage in the interphase region (Fard *et al*. 2020).

5. Conclusions

Utilizing state-of-the-art PFQNM as well as with FV and FFV, the elastic moduli of a PDMS sample has been evaluated in a time-dependent fashion. Specifically, rigorous calibrations are done. Force data are fitted with a linearized DMT contact mechanics model considering surface adhesion force. Elastic Young's modulus was measured at frequencies spanned four orders of magnitude. The robust local probing of mechanical measurement as well as unprecedented high-resolution topography imaging open new avenues for quantitative nanomechanical mapping of soft polymers, and can be extended to soft biological systems.

- Increased Young's modulus was discovered with increasing acquisition frequency. The Young's modulus is 878 ± 274 kPa at 0.1 Hz but increases to 4586 ± 758 kPa at 2 kHz.
- The acquisition frequency dependent modulus change could be described by a power function $E = 1192.88 \times f^{0.18}$ ($R^2 = 0.99$). Energy dissipation in the range of 0.125 kHz to 2 kHz further supports this observation.

The robust local probing of mechanical measurement as well as unprecedented high-resolution topography imaging open new avenues for quantitative nanomechanical mapping of soft polymers, and can be extended to soft biological systems.

Acknowledgments

The research described in this paper was financially supported by the Natural Science Foundation of China 21807026.

References

Adamcik, J., Berquand, A. and Mezzenga, R. (2011), "Single-step direct measurement of amyloid fibrils stiffness by peak force quantitative nanomechanical atomic force microscopy", *Appl. Phys. Lett.*, **98**, 193701. https://doi.org/10.1063/1.3589369.

Bensaid, I. (2017), "A refined nonlocal hyperbolic shear deformation beam model for bending and dynamic analysis of nanoscale beams", *Adv. Nano Res., Int. J.*, **5**(2), 113-126. https://doi.org/10.12989/anr.2017.5.2.113.

Binnig, G., Quate, C.F. and Gerber, C. (1986), "Atomic force microscope", *Phys. Rev. Lett.*, **56**, 930-933. https://doi.org/10.1103/PhysRevLett.56.930.

Brown, X.Q., Ookawa, K. and Wong, J.Y. (2005), "Evaluation of polydimethylsiloxane scaffolds with physiologically-relevant elastic moduli: Interplay of substrate mechanics and surface chemistry effects on vascular smooth muscle cell response", *Biomaterials*, **26**(16), 3123-3129. https://doi.org/10.1016/j.biomaterials.2004.08.009.

Cao, Y., Yang, D. and Soboyejoy, W. (2005), "Nanoindentation method for determining the initial contact and adhesion characteristics of soft polydimethylsiloxane", *J. Mater. Res.*, **20**(8), 2004-2011. https://doi.org/10.1557/JMR.2005.0256.

Carl, P. and Schillers, H. (2008), "Elasticity measurement of living cells with an atomic force microscope: Data acquisition and processing", *Pflügers Arch.*, **457**, 551. https://doi.org/10.1007/s00424-008-0524-3.

Carrillo, F., Gupta, S., Balooch, M., Marshall, S.J., Marshall, G.W., Pruitt, L. and Puttlitz, C.M. (2005), "Nanoindentation of polydimethylsiloxane elastomers: Effect of crosslinking, work of adhesion, and fluid environment on elastic modulus", *J. Mater. Res.*, **20**, 2820-2830. https://doi.org/10.1557/JMR.2005.0354.

Chuah, Y.J., Koh, Y.T., Lim, K., Menon, N.V., Wu, Y. and Kang, Y. (2015), "Simple surface engineering of polydimethylsiloxane with polydopamine for stabilized mesenchymal stem cell adhesion and multipotency", *Sci. Rep.*, **5**, 18162. https://doi.org/10.1038/srep18162.

Cortese, B., D'Amone, S., Manca, M., Viola, I., Cingolani, R. and Gigli, G. (2008), "Superhydrophobicity due to the hierarchical scale roughness of PDMS surfaces", *Langmuir*, **24**, 2712-2718. https://doi.org/10.1021/la702764x.

Dimitriadis, E.K., Horkay, F., Maresca, J., Kachar, B. and Chadwick, R.S. (2002), "Determination of elastic moduli of thin layers of soft material using the atomic force microscope", *Biophys. J.*, **82**, 2798-2810. https://doi.org/10.1016/S0006-3495(02)75620-8.

Ebrahimi, F., Seyfi, A. and Dabbagh, A. (2019), "Dispersion of waves in FG porous nanoscale plates based on NSGT in thermal environment", *Adv. Nano Res., Int. J.*, **7**(5), 325-335. https://doi.org/10.12989/anr.2019.7.5.325.

Efremov, Y.M., Shpichka, A., Kotova, S. and Timashev, P. (2019), "Viscoelastic mapping of cells based on fast force volume and peak force tapping", *Soft Matter*, **15**, 5455-5463. https://doi.org/10.1039/C9SM00711C.

Eltaher, M.A., Almalki, T.A., Ahmed, K.I. and Almitani, K.H. (2019), "Characterization and behaviors of single walled carbon nanotube by equivalent-continuum mechanics approach", *Adv. Nano Res., Int. J.*, **7**(1), 39-49. https://doi.org/10.12989/anr.2019.7.1.039.

Fard, M.Y., Raji, B. and Pankretz, H. (2020), "Time-scale through-thickness interphase in polymer matrix composites including hygrothermal treatment", *Polym. Test.*, **83**, 106365. https://doi.org/10.1016/j.polymertesting.2020.106365.

Fujii, T. (2002), "PDMS-based microfluidic devices for biomedical applications", *Microelec. Eng.*, **61**, 907-914. https://doi.org/10.1016/S0167-9317(02)00494-X.

Germanicus, R.C., Mercier, D., Agrebi, F., Fèbvre, M., Mariolle, D., Descamps, P. and Leclère, P. (2020), "Quantitative mapping of high modulus materials at the nanoscale: Comparative study between atomic force microscopy and nanoindentation", *J. Microsc.*, **280**, 51-62. https://doi.org/10.1111/jmi.12935.

Hellwig, J., Karlsson, R.M., Wågberg, L. and Pettersson, T. (2017), "Measuring elasticity of wet cellulose beads with an AFM colloidal probe using a linearized DMT model", *Anal. Methods*, **9**, 4019-4022. https://doi.org/10.1039/C7AY01219E.

Johnston, I., McCluskey, D., Tan, C. and Tracey, M. (2014), "Mechanical characterization of bulk Sylgard 184 for microfluidics and microengineering", *J. Micromech. Microeng.*, **24**, 035017. https://doi.org/10.1088/0960-1317/24/3/035017.

Kang, L., Smith, S. and Wang, C. (2019), "Metal-organic framework preserves the biorecognition of antibodies on nanoscale surfaces validated by single-molecule force spectroscopy", *ACS Appl. Mater. Interf.*, **12**, 3011-3020. https://doi.org/10.1021/acsami.9b19551.

Kim, H.J., Matsuda, H., Zhou, H. and Honma, I. (2006), "Ultrasound-triggered smart drug release from a poly (dimethylsiloxane)-mesoporous silica composite", *Adv. Mater.*, **18**, 3083-3088. https://doi.org/10.1002/adma.200600387

Kim, K.S., Lin, Z., Shrotriya, P., Sundararajan, S. and Zou, Q. (2008), "Iterative control approach to high-speed force-distance curve measurement using AFM: Time-dependent response of PDMS example", *Ultramicroscopy*, **108**, 911-920. https://doi.org/10.1016/j.ultramic.2008.03.001.

Krieg, M., Fläschner, G., Alsteens, D., Gaub, B.M., Roos, W.H., Wuite, G.J., Gaub, H.E., Gerber, C., Dufrene, Y.F. and Muller, D.J. (2019), "Atomic force microscopy-based mechano-biology", *Nat. Rev. Phys.*, **1**, 41-57. https://doi.org/10.1038/s42254-018-0001-7

Lee, J.N., Park, C. and Whitesides, G.M. (2003), "Solvent compatibility of poly (dimethylsiloxane)-based microfluidic devices", *Anal. Chem.*, **75**, 6544-6554. https://doi.org/10.1021/ac0346712.

Liu, M., Sun, J., Sun, Y., Bock, C. and Chen, Q. (2009), "Thickness-dependent mechanical properties of polydimethyl-siloxane membranes", *J. Micromech. Microeng.*, **19**, 035028. https://doi.org/10.1088/0960-1317/19/3/035028.

Liu, S., Gordiichuk, P., Wu, Z.S., Liu, Z., Wei, W., Wagner, M., Mohamed-Noriega, N., Wu, D., Mai, Y., Herrmann, A., Mullen, K. and Feng, X. (2015), "Patterning two-dimensional free-standing surfaces with mesoporous conducting polymers", *Nat. Commun.*, **6**, 1-9. https://doi.org/10.1038/ncomms9817.

Mata, A., Fleischman, A.J. and Roy, S. (2005), "Characterization of polydimethylsiloxane (PDMS) properties for biomedical micro/nanosystems", *Biomed. Microdev.*, **7**, 281-293. https://doi.org/10.1007/s10544-005-6070-2.

McDonald, J.C. and Whitesides, G.M. (2002), "Poly (dimethyl-lsiloxane) as a material for fabricating microfluidic devices", *Acc. Chem. Res.*, **35**(7), 491-499. https://doi.org/10.1021/ar010110q.

Piruska, A., Nikcevic, I., Lee, S.H., Ahn, C., Heineman, W.R., Limbach, P.A. and Seliskar, C.J. (2005), "The autofluorescence of plastic materials and chips measured under laser irradiation", *Lab Chip*, **5**, 1348-1354. https://doi.org/10.1039/B508288A.

Punjabi, K., Mehta, S., Yedurkar, S., Jain, R., Mukherjee, S., Kale, A. and Deshpande, S. (2018), "Extracellular synthesis of silver nanoparticle by pseudomonas hibiscicola-mechanistic approach", *Adv, Nano Res., Int. J.*, **6**(1), 81-92. https://doi.org/10.12989/anr.2018.6.1.081.

Reyes, O., Sanchez, M.F., Pal, M., Llorca, J. and Sebastian, P. (2017), "Evolution pathway of CZTSe nanoparticles synthesized by microwave-assisted chemical synthesis", *Adv. Nano Res., Int. J.*, **5**(3), 203-214. https://doi.org/10.12989/anr.2017.5.3.203.

Sarrazin, B., Brossard, R., Guenoun, P. and Malloggi, F. (2016), "Investigation of PDMS based bi-layer elasticity via interpretation of apparent Young's modulus", *Soft Matter*, **12**, 2200-2207. https://doi.org/10.1039/C5SM02133B.

Schillers, H., Medalsy, I., Hu, S., Slade, A.L. and Shaw, J.E. (2016), "Peakforce tapping resolves individual microvilli on living cells", *J. Mol. Recognit.*, **29**, 95-101. https://doi.org/10.1002/jmr.2510.

Shi, X. and Zhao, Y.P. (2004), "Comparison of various adhesion contact theories and the influence of dimensionless load parameter", *J. Adhes. Sci. Technol.*, **18**, 55-68. https://doi.org/10.1163/156856104322747009.

Sia, S.K. and Whitesides, G.M. (2003), "Microfluidic devices fabricated in poly (dimethylsiloxane) for biological studies", *Electrophoresis*, **24**, 3563-3576. https://doi.org/10.1002/elps.200305584.

Supraja, N., Dhivya, J., Prasad, T. and David, E. (2018), "Synthesis, characterization and dose dependent antimicrobial and anticancerous efficacy of phycogenic (Sargassum muticum) silver nanoparticles against breast cancer cells (MCF 7) cell line", *Adv. Nano Res., Int. J.*, **6**(2), 183-200. https://doi.org/10.12989/anr.2018.6.2.183.

Trtik, P., Kaufmann, J. and Volz, U. (2012), "On the use of peak-force tapping atomic force microscopy for quantification of the local elastic modulus in hardened cement paste", *Cem. Concrete Res.*, **42**, 215-221. https://doi.org/10.1016/j.cemconres.2011.08.009.

Vahdat, V., Grierson, D.S., Turner, K.T. and Carpick, R.W. (2013), "Mechanics of interaction and atomic-scale wear of amplitude modulation atomic force microscopy probes", *ACS Nano*, **7**, 3221-3235. https://doi.org/10.1021/nn305901n.

Villanueva-Cab, J. and Pal, U. (2017), "Evaluation of thermally and chemically reduced graphene oxide films as counter electrodes on dye-sensitized solar cells", *Adv. Nano Res., Int. J.*, **5**(3), 231-244. https://doi.org/10.12989/anr.2017.5.3.231.

Wang, Z., Volinsky, A.A. and Gallant, N.D. (2015), "Nano-indentation study of polydimethylsiloxane elastic modulus using B erkovich and flat punch tips", *J. Appl. Polym. Sci.*, **132**, 41384. https://doi.org/10.1002/app.41384.

Wu, J., Wang, R., Yu, H., Li, G., Xu, K., Tien, N.C., Roberts, R.C. and Li, D. (2015), "Inkjet-printed microelectrodes on PDMS as biosensors for functionalized microfluidic systems", *Lab Chip*, **15**, 690-695. https://doi.org/10.1039/C4LC01121J.

Xin, C., Chen, L., Li, T., Zhang, Z., Zhao, T., Li, X. and Zhang, J. (2018), "Highly sensitive flexible pressure sensor by the integration of microstructured PDMS film with a-IGZO TFTs", *IEEE Electron. Device Lett.*, **39**, 1073-1076. https://doi.org/10.1109/LED.2018.2839595.

Xu, K., Sun, W., Shao, Y., Wei, F., Zhang, X., Wang, W. and Li, P. (2018), "Recent development of peakforce tapping mode atomic force microscopy and its applications on nanoscience", *Nanotechnol. Rev.*, **7**, 605-621. https://doi.org/10.1515/ntrev-2018-0086.

Young, T., Monclus, M., Burnett, T., Broughton, W., Ogin, S. and Smith, P. (2011), "The use of the peakforce^{TM} quantitative nanomechanical mapping AFM-based method for high-resolution Young's modulus measurement of polymers", *Meas. Sci. Technol.*, **22**, 125703. https://doi.org/10.1088/0957-0233/22/12/125703.

Zeng, G., Dirscherl, K. and Garnæs, J. (2018), "Toward accurate quantitative elasticity mapping of rigid nanomaterials by atomic force microscopy: effect of acquisition frequency, loading force, and tip geometry", *Nanomaterials*, **8**, 616. https://doi.org/10.3390/nano8080616.

Ziaie, B., Baldi, A., Lei, M., Gu, Y. and Siegel, R.A. (2004), "Hard and soft micromachining for BioMEMS: Review of techniques and examples of applications in microfluidics and drug delivery", *Adv. Drug Deliv. Rev.*, **56**, 145-172. https://doi.org/10.1016/j.addr.2003.09.001.

JL